Modeling Niemann–Pick disease type C in a human haploid cell line allows for patient variant characterization and clinical interpretation

Steven Erwood, Reid A. Brewer, Teija M.I. Bily, et al.

Genome Res. 2019 29: 2010-2019 originally published online November 21, 2019
Access the most recent version at doi:10.1101/gr.250720.119

Method

Modeling Niemann–Pick disease type C in a human haploid cell line allows for patient variant characterization and clinical interpretation

Steven Erwood,[1,2] Reid A. Brewer,[1] Teija M.I. Bily,[1] Eleonora Maino,[1,2] Liangchi Zhou,[1] Ronald D. Cohn,[1,2,3] and Evgueni A. Ivakine[1]

[1]*Program in Genetics and Genome Biology, The Hospital for Sick Children Research Institute, Toronto, Ontario, M5G 0A4, Canada;* [2]*Department of Molecular Genetics, University of Toronto, Toronto, Ontario, M5S 1A8, Canada;* [3]*Department of Pediatrics, University of Toronto and The Hospital for Sick Children, Toronto, Ontario, M5G 1X8, Canada*

The accurate clinical interpretation of human sequence variation is foundational to personalized medicine. This remains a pressing challenge, however, as genome sequencing becomes routine and new functionally undefined variants rapidly accumulate. Here, we describe a platform for the rapid generation, characterization, and interpretation of genomic variants in haploid cells focusing on Niemann–Pick disease type C (NPC) as an example. NPC is a fatal neurodegenerative disorder characterized by a lysosomal accumulation of unesterified cholesterol and glycolipids. In 95% of cases, NPC is caused by mutations in the *NPC1* gene, for which more than 200 unique disease-causing variants have been reported to date. Furthermore, the majority of patients with NPC are compound heterozygotes that often carry at least one private mutation, presenting a challenge for the characterization and classification of individual variants. Here, we have developed the first haploid cell model of NPC. This haploid cell model recapitulates the primary biochemical and molecular phenotypes typically found in patient-derived fibroblasts, illustrating its utility in modeling NPC. Additionally, we show the power of CRISPR/Cas9-mediated base editing in quickly and efficiently generating haploid cell models of individual patient variants in NPC. These models provide a platform for understanding the disease mechanisms underlying individual *NPC1* variants while allowing for definitive clinical variant interpretation for NPC.

[Supplemental material is available for this article.]

Niemann–Pick disease type C (NPC) is a rare autosomal recessive lysosomal storage disorder affecting one in 90,000 individuals (Vanier 2010; Wassif et al. 2016). In 95% of cases, NPC is caused by mutations in the gene *NPC1*, which is required for the proper transport of sterols from the lysosome to other subcellular compartments (Vanier 2010). Although NPC is a clinically heterogeneous disorder with symptoms ranging from hepatosplenomegaly to ataxia and seizures, the disease is defined by fatally progressive neurodegeneration (Vanier 2010; Patterson et al. 2013). These symptoms are caused by the intracellular accumulation of cholesterol and glycolipids within late endosomes and lysosomes (Ory 2000; Wojtanik and Liscum 2003). This accumulation is easily visualized in patient-derived fibroblasts using a fluorescent dye called filipin, which is used as a primary assay in the diagnosis of NPC (McKay Bounford and Gissen 2014).

More than 200 disease-causing mutations have been identified in *NPC1* that define a heterogeneous mutational spectrum that includes missense and nonsense mutations, small duplication, deletion and insertion mutations, and splice-site mutations (Millat et al. 2001; Tarugi et al. 2002; Park et al. 2003; Scott and Ioannou 2004; Fernandez-Valero et al. 2005). The primary source material used to understand NPC pathology in humans is patient-derived fibroblasts (Greer et al. 1999; Millat et al. 2001; Yamamoto et al. 2004; Gelsthorpe et al. 2008; Zampieri et al. 2012; Rauniyar et al. 2015). The majority of patients with NPC, however, present as compound heterozygotes that often harbor at least one private mutation. This presents a challenge in understanding the molecular mechanisms of disease underlying individual *NPC1* variants, leaving most documented mutations as variants of uncertain significance. Further complicating variant interpretation, it has been shown that variant pathogenicity is contingent on level of expression. Specifically, certain variants that are pathogenic at physiologically relevant expression levels can rescue disease phenotypes when artificially overexpressed (Gelsthorpe et al. 2008; Zampieri et al. 2012).

The advent of CRISPR/Cas9-based genome editing has allowed for modifications to genomes with a precision and efficiency unparalleled by previous technologies (Mali et al. 2013a). In brief, CRISPR/Cas9-based genome editing relies on a guide RNA programmable bacterial endonuclease, Cas9, to induce a targeted DNA double-stranded break (DSB). In the absence of a repair template, this break is predominantly repaired by nonhomologous end joining (NHEJ), which is stochastic and leads to small insertions or deletions (Jinek et al. 2012; Cho et al. 2013; Mali et al. 2013b). Typically, even when a repair template is exogenously supplied, NHEJ is responsible for the majority of genome editing outcomes with CRISPR/Cas9, making the establishment of models with specifically designed modifications inefficient. Recently,

Corresponding author: zhenya.ivakine@sickkids.ca
Article published online before print. Article, supplemental material, and publication date are at http://www.genome.org/cgi/doi/10.1101/gr.250720.119.

29:2010–2019 Published by Cold Spring Harbor Laboratory Press; ISSN 1088-9051/19; www.genome.org

this challenge has been addressed with the introduction of CRISPR/Cas9-mediated base editing, which uses a nucleobase deaminase enzyme fused to a catalytically impaired Cas9 enzyme capable of inducing only single-stranded breaks (Rees and Liu 2018). These nucleobase deaminase enzymes, APOBEC1 and TadA for cytosine and adenine base editing, respectively, operate on single-stranded DNA (ssDNA), exclusively (Komor et al. 2016; Gaudelli et al. 2017). Similar to traditional CRISPR/Cas9-based genome editing, this fusion protein can be targeted to a guide RNA–specified genomic locus. When the guide RNA binds to its target sequence, the complementary strand is displaced, becoming available for modification by the deaminase enzyme (Nishimasu et al. 2014). In practice, only a portion of the displaced "R loop" is prone to deamination with the current generation of CRISPR/Cas9 base editors, corresponding to an ~5-bp editing window located 13–17 bp upstream of the protospacer-adjacent motif sequence (PAM) (Komor et al. 2016; Gaudelli et al. 2017; Rees et al. 2017). Deamination of cytosine produces uridine, which base pairs as thymidine, whereas deamination of adenosine produces inosine, which has base-pairing preferences equivalent to guanosine (Yasui et al. 2008). The single-stranded nick produced on the unedited strand by the Cas9 enzyme then induces endogenous DNA repair pathways that will use the edited strand as a template, effectuating either a C•G-to-T•A or an A•T-to-G•C base pair transition.

Here, we aimed to show that by CRISPR/Cas9-mediated *NPC1* gene editing, the HAP1 cell line, a human near-haploid cell line, can serve as an effective model of NPC. By doing so, we present a highly efficient approach to resolve the clinical interpretations of *NPC1* variants that extends to those both seen and not yet seen in the clinic.

Results

Generation and characterization of an *NPC1*-deficient near-haploid cell line

As NPC is an autosomal recessive disorder, cellular disease modeling requires the disruption of each allele present in the target cell type. This presents a challenge given the diploid or often aneuploid nature of typical human cell lines, especially if uniform allele disruption is desired. HAP1 cells, however, are a near-haploid human cell line containing a single copy of each chromosome, with the exception of a heterozygous fragment of Chromosome 15, making them an excellent system for loss-of-function disease modeling (Carette et al. 2011). We used CRISPR/Cas9-mediated gene targeting to generate *NPC1*-deficient HAP1 cells. To disrupt *NPC1* expression, we selected several single guide RNAs (sgRNAs) with minimal computationally predicted off-target activity that target exon 21 of the *NPC1* locus. These sgRNAs were cloned into plasmids, allowing coexpression with *Streptococcus pyogenes* Cas9 (SpCas9), and tested for editing efficiency. The two most highly active sgRNAs were transfected separately into wild-type HAP1 cells (Fig. 1A; Supplemental Table S1). Following 72 h of antibiotic selection to enrich for successfully transfected cells, isogenic clones were isolated by limited dilution and screened by Sanger sequencing for locus disruption. Out of 15 clones screened, six isogenic cell clones were identified with unique mutations in the targeted locus, and three clones were carried forward for further characterization. A 28-bp deletion was detected in the first clone (NCBI reference sequence: NG_012795.1 *NPC1*: g.54927_54954del), resulting in a frame-shift and the formation of a premature stop codon six amino acids downstream from the deletion site (Fig. 1B). The second clone (NG_012795.1 *NPC1*: g.54902insA) harbored an insertion of an adenine nucleotide at the predicted DSB site, resulting in a frameshift and the formation of a premature stop codon four amino acids downstream from the insertion (Fig. 1C). The third clone (NG_012795.1 *NPC1*: g.54899_54904del) contained an in-frame 6-bp deletion (Fig. 1D). To assess whether these mutations were sufficient to disrupt NPC1 expression, we performed a western blot for NPC1 protein. Both clones with frameshift mutations showed a complete absence of NPC1 protein, whereas the third clone showed residual protein expression and appeared to run as a doublet, with a second band at a slightly lower molecular weight (Fig. 1E). For the first two clones, this indicates that both frameshift mutations are sufficient in generating null *NPC1* alleles. In the third clone, the doublet staining of NPC1 likely indicates a heterogeneously glycosylated protein product, a phenomenon that has been previously reported for a variety of NPC variants (Watari et al. 1999; Zampieri et al. 2012; Nakasone et al. 2014), and the reduced expression indicates that perturbations to the *NPC1* locus, in spite of a preserved reading frame, can negatively influence protein expression. Our three cell clones, with their disrupted NPC1 protein expression, represent the first haploid cell models of NPC.

A hallmark biochemical feature of NPC pathology is the accumulation of unesterified cholesterol and glycolipids within late endosomes and lysosomes. Presently, the demonstration of defective intracellular cholesterol transport and homeostasis is considered the most definitive functional diagnostic test for NPC (McKay Bounford and Gissen 2014). This defect is readily visualized in NPC patient fibroblasts by staining with the fluorescent compound filipin, which stains unesterified cholesterol deposits (Supplemental Fig. S1). We assessed whether the *NPC1*-deficient HAP1 cells displayed a similar biochemical phenotype using filipin staining. All three cell clones display distinct foci of intracellular filipin staining that are absent in unedited HAP1 cells, indicative of impaired trafficking of unesterified cholesterol in the *NPC1*-deficient HAP1 cells (Fig. 1F). The development of disease-relevant pathology in *NPC1*-deficient HAP1 cell clones shows the potential of these cells in understanding disease mechanisms in NPC.

Modeling *NPC1* variants in a haploid cell model using CRISPR / Cas9-mediated base editing

After showing the effectiveness of HAP1 cells in recapitulating a primary cellular phenotype of NPC, we sought to investigate the feasibility of modeling individual *NPC1* variants using HAP1 cells. To do this, we elected to use CRISPR/Cas9-mediated base editing. CRISPR/Cas9-mediated base editing technologies are capable of targeted single-nucleotide transitions within a designated editing-window upstream of the PAM sequence (Komor et al. 2016; Gaudelli et al. 2017). We selected mutations that span the NPC1 protein and that are representative of the *NPC1* mutation spectrum, including missense, nonsense, and synonymous mutations and a splice site mutation. We selected variants that have or have not been previously documented in clinical databases, as well as variants of both known and unknown pathogenicity. The 19 variants modeled are documented in Table 1. Although we focused on the C-terminal luminal loop domain, spanning residues 855–1098 of NPC1, where 45% of NPC patient mutations occur (Greer et al. 1999; Li et al. 2017), we selected sgRNAs to establish at least one mutation in each of five functional protein domains (Davies and Ioannou 2000). These sgRNA cassettes were cloned into a U6-driven expression vector and individually cotransfected into wild-type

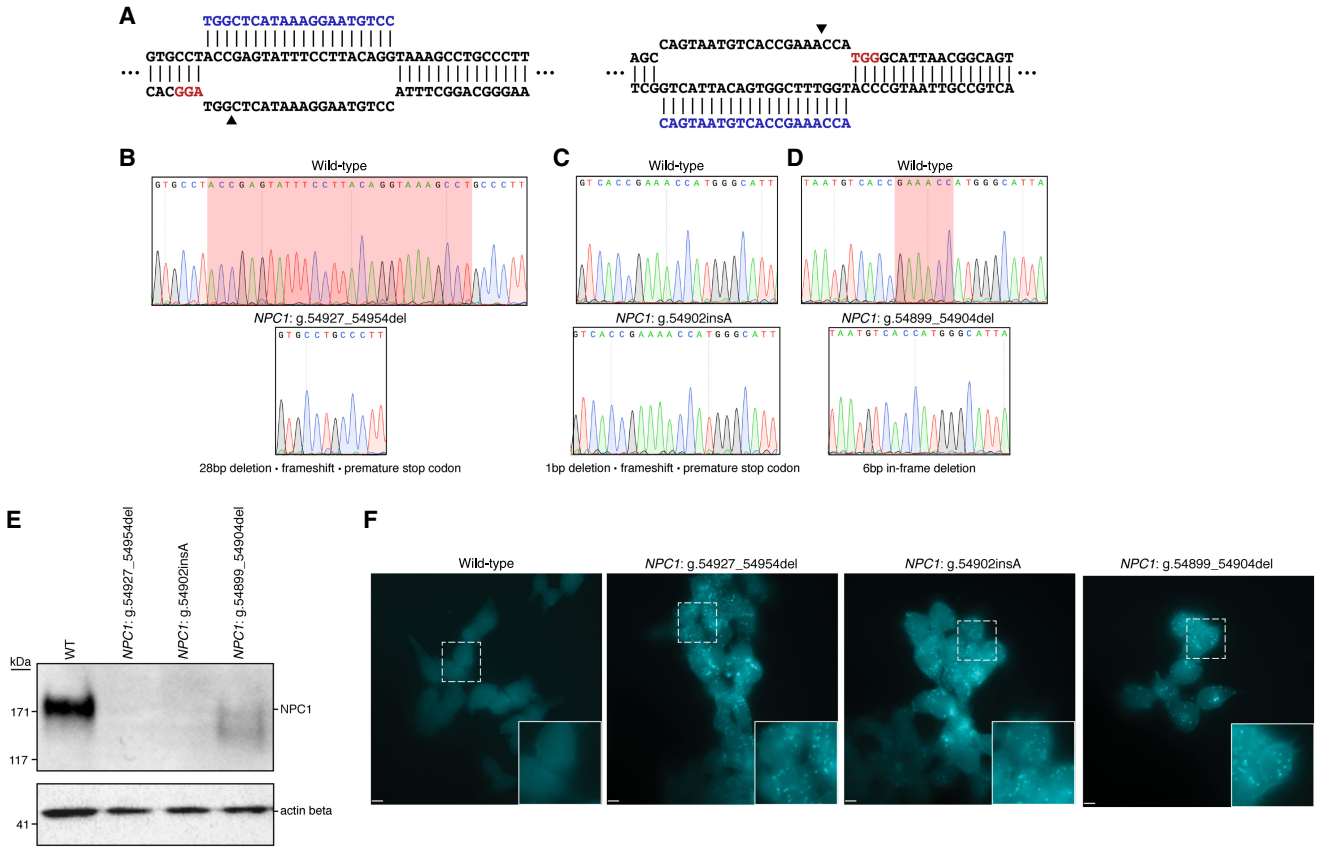

Figure 1. Generation and characterization of three haploid models of Niemann–Pick disease type C (NPC). (*A*) Diagrams illustrating the two targeted sites in *NPC1*. Arrowheads indicate the predicted DSB site. (*B–D*) Sequencing chromatographs showing wild-type *NPC1* (*top*) and the specific disruption in each isogenic edited cell clone (*bottom*). (*B,D*) Red highlighted region indicates the locations of the deletions in edited clones. (*C*) Red highlighted region indicates the position of the insertion in the edited clone. (*E*) Western blot analysis from total protein lysate from wild-type HAP1 cells and the three edited cell clones illustrating absent or reduced NPC1 protein expression. Actin beta was used as a loading control. (*F*) Filipin staining reveals deposits of intracellular cholesterol in edited cells that are absent in wild-type cells. White dashed-bordered box has been enlarged twofold and *inset* at *bottom right*. Scale bars, 6.3 μm.

HAP1 cells alongside either a Cas9 cytosine or adenine base editor plasmid (Koblan et al. 2018; Nishimasu et al. 2018; Zafra et al. 2018; Huang et al. 2019). Following antibiotic selection, transfected cells were subject to limited dilution to isolate isogenic clones. In each case, editing was apparent in a bulk population, ranging from 10% to 48% (Supplemental Fig. S2). When clones were individually screened by Sanger sequencing by analyzing the genomic sequence ranging from at least 100 bp both upstream of and downstream from the sgRNA binding site, between 8% and 60% of isogenic clones were positively edited (Table 1). Our system for model generation resulted in clonal isolation in just >2 wk with an average frequency of positive clone-selection of ~27% (Table 1; Fig. 2A). The editing in all but two of the 19 variants isolated was contained to a single codon. During the generation of the NPC1 p.R1077X variant, the editing window contained a second cytosine adjacent to the targeted cytosine, and in our screened clones, we were only able to identify clones in which both bases were edited. The secondary mutation, however, is a silent mutation in which the adjacent histidine codon has been changed from TAC to TAT, resulting in an NPC1 p.Y1076=/R1077X cell line (hereafter referred to as NPC1 p.R1077X) (Supplemental Fig. S3). Similarly, when isolating the NPC1 p.I1061T variant, an adjacent adenine two bases upstream was uniformly targeted in all edited clones, resulting in a secondary silent mutation and an NPC1 p.L1060=/I1061T cell line (hereafter referred to as NPC1 p.I1061T). For the rest of the *NPC1* variants, however, multiple clones were isolated with editing contained to a single codon (Table 1; Supplemental Fig. S3). These data show that both CRISPR/Cas9-mediated cytosine and adenine base editing are highly efficient in HAP1 cell model generation, providing a viable solution to the documented poor efficiency of introducing single-nucleotide variants (SNVs) by typical CRISPR/Cas9-based homology-directed repair, which is particularly inefficient in HAP1 cells (Findlay et al. 2018).

Haploid cell models of *NPC1* variants allow for variant characterization and clinical interpretation

The majority of NPC patients are compound heterozygotes and often carry at least one private mutation (Park et al. 2003; Fernandez-Valero et al. 2005). As a consequence, it remains challenging to attribute a specific molecular mechanism of disease to an individual *NPC1* variant. By using our haploid models, we sought to characterize the 19 aforementioned *NPC1* variants. First, we assayed the expression of *NPC1* mRNA in four of the cell models—NPC1 p.D945N, NPC1 p.R1077X, NPC1 p.D1097N and *NPC1* c.3591+2T>C—in which variant interpretation has

Table 1. Summary of *NPC1* mutations modeled

Variant	Editor	Nucleotide change	ClinVar annotation	Functional outcome observed	Positive clones (%)
NPC1 p.R4H	SpCas9-NG Target-AID	CGC > CAC	*Undocumented*	Benign	8
NPC1 p.F402P	SpCas9 ABEmax	TTC > CCC	*Undocumented*	Pathogenic	15
NPC1 p.F402S	SpCas9 ABEmax	TTC > TCC	*Undocumented*	Pathogenic	43
NPC1 p.E406G	SpCas9 ABEmax	GAG > GGG	*Undocumented*	Pathogenic	33
NPC1 p.Y634Y	SpCas9 ABEmax	TAT > TAC	*Undocumented*	Benign	10
NPC1 p.Y634C	SpCas9 ABEmax	TAT > TGT	*Variant of uncertain significance*	Pathogenic	10
NPC1 p.I635T	SpCas9 ABEmax	ATT > ACT	*Undocumented*	Benign	15
NPC1 p.G765K	SpCas9-NG Target-AID	GGA > AAA	*Undocumented*	Pathogenic	14
NPC1 p.L785S	NG-Cas9 ABEmax	TTA > TCA	*Undocumented*	Pathogenic	60
NPC1 p.D898N	SpCas9 CBE	GAC > AAC	*Variant of uncertain significance*	Pathogenic	50
NPC1 p.D945N	SpCas9 CBE	GAT > AAT	*Variant of uncertain significance*	Pathogenic	43
NPC1 p.L1060P	NG-Cas9 ABEmax	CTT > CCC	*Undocumented*	Pathogenic	60
NPC1 p.L1060=, I1061T	VRQR-SpCas9 ABEmax	CTT ATA > CTC ACA	*Pathogenic*	Pathogenic	8
NPC1 p.Y1076=, R1077X	SpCas9 CBE	TAC CGA > TAT TGA	*Pathogenic*	Pathogenic	21
NPC1 p.D1097N	SpCas9 CBE	GAC > AAC	*Likely pathogenic*	Pathogenic	20
NPC1 p.V1158=	SpCas9 CBE	GTG > GTA	*Undocumented*	Benign	21
NPC1 p.M1159T	SpCas9 ABEmax	ATG > ACG	*Undocumented*	Benign	27
NPC1 c.3591+2 T>C	SpCas9 ABEmax	GTG > GCG	*Likely pathogenic*	Pathogenic	25
NPC1 p.Y1267C	VRQR-Cas9 ABEmax	TAC > TGC	*Undocumented*	Benign	33

been previously documented. Although there was a trend toward increased *NPC1* mRNA expression in NPC1 p.D945N, NPC1 p.D1097N, and *NPC1* c.3591+2T>C compared with the wild type, no measurement reached significance (Fig. 2B). This aligns with previously reported data from NPC patient fibroblasts, in which select missense mutations and in-frame deletion mutations have been shown to result in modestly increased *NPC1* mRNA expression (Yamamoto et al. 2004; Gelsthorpe et al. 2008). In the NPC1 p.R1077X cell model, however, there was a significant reduction in *NPC1* mRNA expression (25.3% ± 14%, $P = 0.002$, $n = 3$) (Fig. 2B). We suspect the reduction in *NPC1* mRNA expression is the result of nonsense mediated decay owing to the introduced premature stop codon, as previously reported for other nonsense variants in NPC and a variety of other genetic disorders (Frischmeyer and Dietz 1999; Macias-Vidal et al. 2009). The modeled splice-site mutation, *NPC1* c.3591+2T>C, is predicted to disrupt canonical splicing of the *NPC1* transcript. To assess splicing, we designed a cDNA-based PCR assay that amplified a region between exons 21 and 25 (Fig. 2C). In our assay, amplification of the *NPC1* c.3591+2T>C splice-site mutation model resulted in a band ~100 bp shorter than the wild-type amplicon (Fig. 2C). By Sanger sequencing, we confirmed that the shorter amplicon was indeed the result of exon 23 (114 bp in length) exclusion (Fig. 2C).

Next, by analyzing NPC1 protein expression via western blot, we found that mutant NPC1 expression varied in apparent molecular weight and level of expression. Six of the 19 variants—NPC1 p.R4H, NPC1 p.F402P, NPC1 p.Y634=, NPC1 p. I635T, NPC1 p.V1158=, and NPC1 p.M1159T—ran with an equivalent molecular weight to wild-type NPC1 protein (Fig. 3). Each of these variants had similar NPC1 expression compared with the wild type, with exception of NPC1 p.F402P, which had a moderate reduction in protein expression. Seven of the 19 variants—NPC1 p.E406G, NPC1 p.Y634C, NPC1 p.G765K, NPC1 p. L1060P, NPC1 p.I1061T, NPC1 p.D1097N, and *NPC1* c.3591+2T>C—ran as a single band at a lower molecular weight than wild-type NPC1 protein (Fig. 3) and showed reduced expression compared with the wild type. Of note, the reduction in protein expression found in the *NPC1* c.3591+2T>C implies that despite the exon 23 exclusion leaving the open reading frame intact, the protein is likely being targeted for degradation. Four of the 19 variants—NPC1 p.F402S, NPC1 p.L785S, NPC1 p.D898N, and NPC1 p.D945N—showed a reduction in total protein and ran as two bands, one equivalent to the wild type and the other equivalent to that found in the lower-molecular-weight mutants (Fig. 3). The distinct molecular weights found in a subset of the mutant variants modeled is consistent with findings in patient-derived fibroblasts and have been attributed to endoplasmic reticulum–associated protein degradation and heterogeneous glycosylation (Watari et al. 1999; Yamamoto et al. 2000; Millat et al. 2001; Gelsthorpe et al. 2008; Zampieri et al. 2012; Nakasone et al. 2014). The NPC1 p.R1077X model, consistent with the reduced mRNA expression, showed a complete absence of NPC1 protein (Fig. 3). In preliminary assays, the NPC1 p.Y1267C model also displayed a total absence of NPC1 protein (Fig. 3). The amino acid change for this variant, however, occurs within immunogen sequence of the primary C-terminal antibody. Upon further analysis with an N-terminal antibody, we found that the NPC1 p.Y1267C protein ran similarly to the wild type (Supplemental Fig. S4). Having observed different levels of expression and migration patterns in our models, we assayed cholesterol homeostasis in each of the cell lines (Fig. 4; Supplemental Fig. S5). With the exception of NPC1 p.L785S, all variants that ran either as a single lower-molecular-weight band or a doublet showed defective cholesterol trafficking indicated by the distinct foci of cholesterol deposits revealed by filipin staining. Despite a marked reduction in NPC1 protein, the NPC1 p.L785S model appeared largely indistinguishable from wild-type HAP1 cells by filipin staining, with only a minor subset (~5%) of cells showing lysosomal cholesterol accumulation (Fig. 4). It is likely that this variant represents what has been well documented in a minority of NPC patients, a variant biochemical phenotype. In these biochemical variants, filipin staining of patient-derived fibroblasts is less definitive (Vanier et al. 1991). Six of the 19 variants—the two variants harboring silent mutations, NPC1 p.Y634= and NPC1 p.V1158=, and the missense mutants NPC1 p.R4H, NPC1 p.I635T, NPC1 p.M1159T, and NPC1 p.Y1267C—appeared comparable to wild type (Supplemental Fig. S5).

Taken together, these data provide strong functional evidence for the clinical pathogenicity of each variant modeled, summarized in Table 1. Critically, our data resolve the clinical interpretation of three variants presently documented as variants

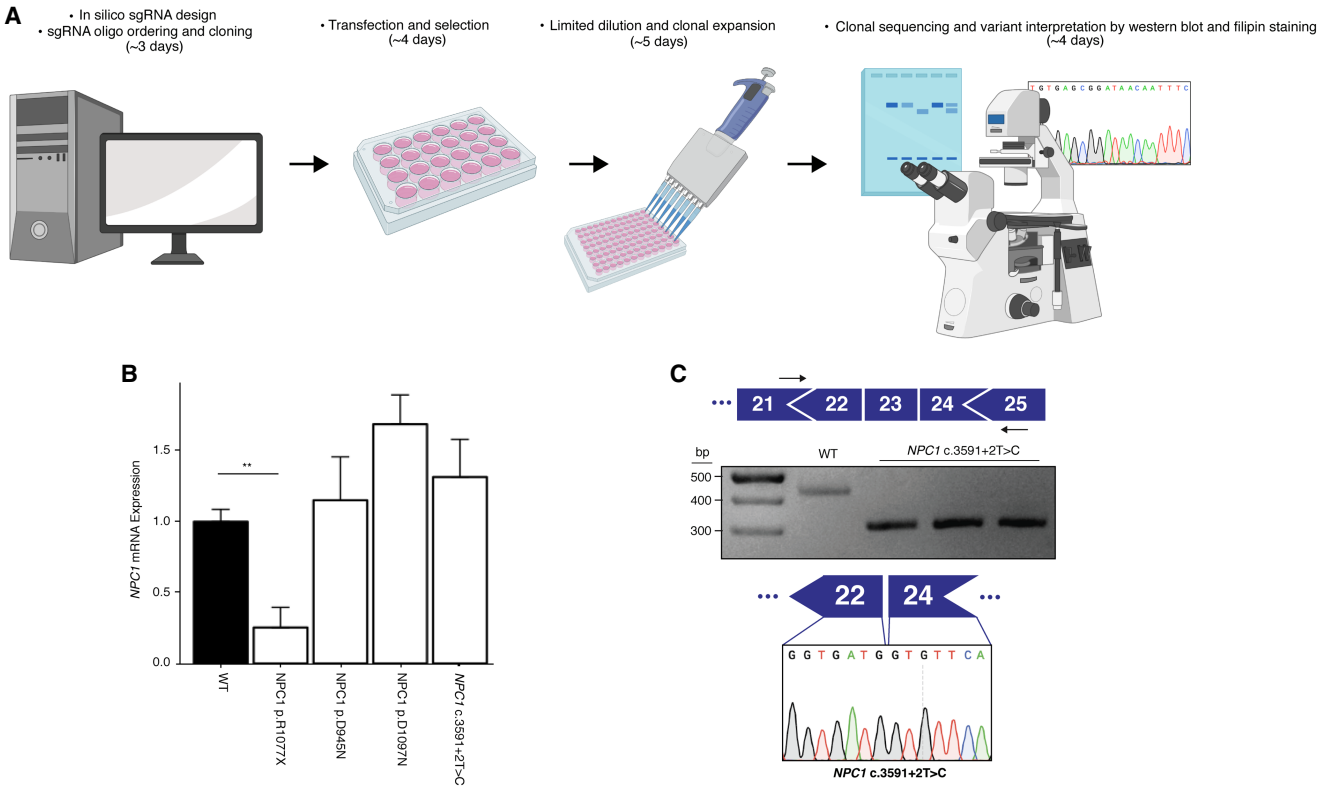

Figure 2. *NPC1* expression in NPC variant cell models. (*A*) Schematic overview of the process of cell model generation and characterization. (*B*) Expression of *NPC1* mRNA is significantly decreased in the NPC1 p.R1077X cell model ($n = 3$, $P = 0.002$ by two-tailed *t*-test) but is unchanged in all other variants assayed. (*C*, *top*) Diagram illustrating PCR assay used to analyze splicing. (*Middle*) PCR amplification results in a shorter amplicon in *NPC1* c.3591 +2T>C cells compared with the wild type. (*Bottom*) Sequencing chromatogram from *NPC1* c.3591+2T>C cells showing exclusion of exon 23.

of uncertain significance—NPC1 p.Y634C, NPC1 p.D898N, and NPC1 p.D945N, indicating that each variant is pathogenic (Landrum et al. 2016). For the remaining variants, we have either confirmed existing clinical interpretations or made the first interpretation of clinical significance. Together, these data show the utility of our haploid models of *NPC1* variants in the delineation of disease mechanisms and the interpretation of clinical variants.

Discussion

By using CRISPR/Cas9-based genome editing, we have developed the first haploid cell model of NPC. Our model recapitulates the primary biochemical and diagnostic phenotype found in patient-derived fibroblasts. Although other human cells lines deficient in *NPC1* expression have been reported (Rodriguez-Pascau et al. 2012; Du et al. 2017; Tharkeshwar et al. 2017; Zhao and Ridgway 2017), these have all been diploid or aneuploid, without established uniform allelic disruption, and NPC1 deficiency confirmed by immunoblotting only. By using CRISPR/Cas9-mediated gene editing, we obtained two unique *NPC1*-null cell models with indels resulting in verified coding frameshifts, and one *NPC1*-deficient cell model containing a 6-bp in-frame deletion. Similar to NPC patient–derived fibroblasts, these models display a distinct defect in cholesterol trafficking, resulting in the accumulation of unesterified cholesterol. To date, greater than 200 disease-causing mutations in *NPC1* have been reported. Accordingly, it is common for NPC patients to be compound heterozygotes, often harboring at least one private mutation. The precise nature of a given

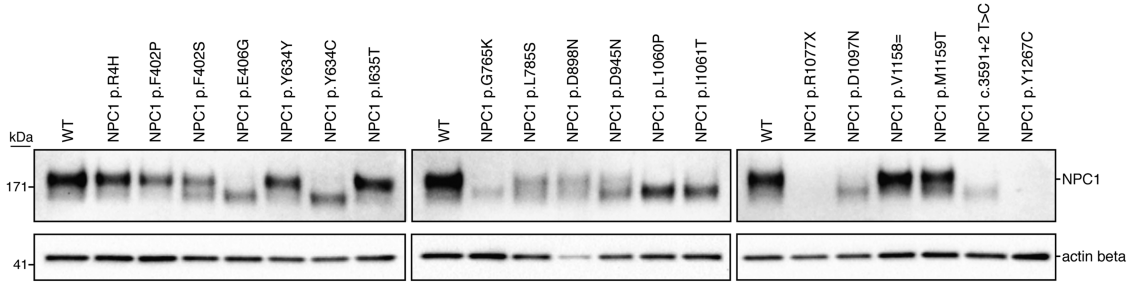

Figure 3. NPC1 expression varies across haploid cell models of NPC. Expression of NPC1 protein was measured via western blot for all *NPC1* variants modeled. Actin beta was used as a loading control.

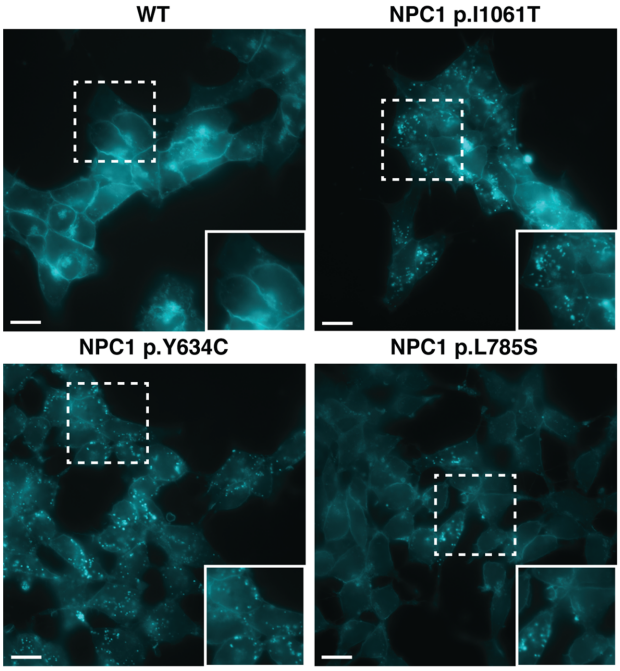

Figure 4. Filipin staining of haploid models of *NPC1* variants. Wild-type (WT) HAP1 cells (*top left*) displayed no defect in cholesterol trafficking. Pathogenic variants, NPC1 p.I1061T and NPC1 p.Y634C (*top right* and *bottom left*, respectively), show distinct foci of filipin staining indicative of a defect in cholesterol trafficking. NPC1 p.L785S (*bottom right*) was found to show a biochemical variant phenotype, with less definitive filipin staining. White dashed-bordered box has been enlarged twofold and *inset* at *bottom right*. Scale bars, 13 μm.

mutation in *NPC1* can vary widely, including both missense and nonsense mutations, splice-site mutations, small duplication mutations, and indel mutations (Millat et al. 2001; Tarugi et al. 2002; Park et al. 2003; Fernandez-Valero et al. 2005). Despite the vast diversity found in the *NPC1* mutation spectrum, most research detailing the molecular mechanisms of NPC have been focused on one mutation, NPC1 p.I1061T (Gelsthorpe et al. 2008; Rauniyar et al. 2015; Schultz et al. 2018). As this allele accounts for between 15% and 20% of all NPC disease alleles (Davies and Ioannou 2000; Millat et al. 2001; Park et al. 2003), it is readily available in homozygous patient fibroblasts, a unique occurrence given the well-documented heterogeneity of *NPC1* mutations. A detailed understanding of the majority of *NPC1* variants using patient-derived fibroblasts, however, remains challenging as they are rarely found in isolation.

Here, we have developed a platform that allows for the rapid generation and analysis of *NPC1* variants. Specifically, our approach allows for the isolation and expansion of mutant cell clones in <14 d. Once established, this system requires only the ordering and cloning of a single pair of oligos encoding a unique sgRNA for each new mutation of interest. By using CRISPR/Cas9-mediated base editing, we modeled 19 unique *NPC1* variants, showing the utility of the system in terms of variant characterization and clinical interpretation and expanding our understanding of the genotype–phenotype relation in *NPC1*. The 19 modeled variants show varied outcomes of *NPC1* mutations at the level of mRNA and protein, suggesting different mechanisms of pathogenicity. As such, our results emphasize the need for a mutation-by-mutation analysis of the *NPC1* gene, which could lead to further insights into basic NPC1 function and help identify unique therapeutic avenues.

CRISPR/Cas9-mediated base editing in HAP1 cells is so efficient that, by screening only a moderate number of clones, one can isolate multiple positive colonies. Recently, two studies have documented off-target editing events as a result of cytosine base editors (Jin et al. 2019; Zuo et al. 2019). It was shown that these off-target events were independent of sgRNA sequence and were enriched in highly transcribed regions. Accordingly, we performed an analysis on three independent cell clones for each variant of interest, minimizing the potential that any observed phenotype to be off-target dependent. Furthermore, we performed RNA sequencing on the parental HAP1 line and nine edited cell clones representing the three biological replicates from three of our modeled variants, NPC1 p.R1077X, NPC1 p.D1097N, and *NPC1* c.3591+2T>C. By using these sequencing reads, we performed variant analysis evaluating the distribution of mutations throughout the cell clones. Although we found between nine to 20 mutations in each clone that were not present in the parental cell line, no single mutation was shared by multiple cell clones indicating that the observed cholesterol accumulation phenotype is independent of potential off-target base editing in the transcriptome (Supplemental Fig. S6A). Additionally, all mutations found were outside of the *NPC1* gene with exception of the desired on-target mutation. Furthermore, of the mutations found there was no apparent bias toward C-to-T or G-to-A substitutions in clones generated using cytosine base editing and no apparent bias toward A-to-G or T-to-C substitutions in clones generated using adenine base editing (Supplemental Fig. S6B). This indicates the mutations observed are unlikely true off-targets but are likely a result of random mutation events.

The American College of Medical Genetics guidelines classify the results of functional assays as strong evidence for or against variant pathogenicity (Richards et al. 2015). We have shown that *NPC1* perturbation leads to a readily visualized defect in cholesterol trafficking in HAP1 cells. This makes haploid models of *NPC1* variants an ideal system for clinical variant interpretation. We showed this by confirming the clinical interpretation of four documented *NPC1* variants, resolving the clinical interpretation of three *NPC1* variants of uncertain significance and establishing the clinical interpretation of 12 presently undocumented *NPC1* variants.

Given the overt phenotype induced by *NPC1* perturbation, it can be envisioned that, if appropriately scaled, a CRISPR/Cas9-mediated base editing screen using HAP1 cells could serve as an effective platform for the clinical interpretation of a multitude of NPC variants. Presently, there are 1839 nonsynonymous *NPC1* mutations documented in the gnomAD database (Lek et al. 2016), 56% of which, are the result of transitional nucleotide substitutions. In the present study, we showed efficient targeting using multiple engineered SpCas9 variants (Table 1). Indeed, with the expanding list of available Cas9 enzymes, each with a unique PAM consensus sequence (Hu et al. 2018; Yang et al. 2018; Hua et al. 2019), it is possible that the vast majority of documented *NPC1* variants could be modeled using CRISPR/Cas9-mediated base editing. Furthermore, base editing systems are not strictly limited to transitional nucleotide substitutions, which further expands their utility in variant interpretation. Although occurring in a less predictable manner, the targeted activation-induced deaminase (AID)-mediated mutagenesis system allows for all nucleotide substitutions of a cytosine (Ma et al. 2016), and the CRISPR-X system allows for all substitutions of both cytosines

and guanines (Hess et al. 2016; Ma et al. 2016). More recently still, it was shown that adenine base editors are capable of cytosine deamination, ultimately resulting in both cytosine-to-guanine or cytosine-to-thymine substitutions (Kim et al. 2019).

Presently, our approach is limited by the editing window of current base editing technologies, which is ~5 bp wide (Komor et al. 2016, 2017; Rees et al. 2017). Although the percentage of total modelable mutations are limited by the currently permissible editing, efforts are underway to engineer enzymes with a much narrower editing window (Tan et al. 2019). We noted at least one editing event with nucleotide substitutions occurring well outside of the predicted editing window for both SpCas9 cytosine and SpCas9 adenine base editors (Supplemental Fig. S3). Although these events were in the minority, they suggest the boundaries of the SpCas9 base editing window are not absolute. Accordingly, it may be possible to design enzymes with a shifted editing window, further expanding the catalog of targetable mutations.

In this study, by using CRISPR/Cas9-mediated gene editing, we have generated and characterized three models of NPC1 deficiency, which represent the first human haploid cell models of NPC. We showed that these models effectively capture the principle diagnostic readout of NPC. The sheer number of *NPC1* variants, combined with most patients being compound heterozygotes, presents a challenge to understanding the disease mechanisms underlying individual patient variants. To overcome this challenge, we sought to model unique *NPC1* variants in HAP1 cells. We showed that this is readily achievable using CRISPR/Cas9-mediated base editing. Finally, we showed that our haploid models of *NPC1* variants allow for efficient variant characterization and clinical interpretation. Although we have focused on NPC, it is worth of note that the largest class of known pathogenic mutations in humans are point mutations (Landrum et al. 2014, 2016). Given the ease and efficiency of our approach, one can envision applying this strategy to a variety of genetic disorders for which a suitable cellular phenotype exists, thus providing a platform for the establishment of detailed genotype–phenotype correlations.

Methods

Cell culture and transfection

HAP1 cells were obtained from Horizon Genomics. HAP1 cells were cultured in Iscove's Modified Dulbecco's Medium (Gibco) supplemented with 10% fetal bovine serum, 1% L-glutamine, and 1% Pen-Strep (Gibco). Patient-derived fibroblasts were cultured in DMEM (Gibco) supplemented with 10% fetal bovine serum, 1% L-glutamine, and 1% Pen-Strep (Gibco). We seeded 500,000 HAP1 cells for transfection in 2 mL of media in six-well plates using Lipofectamine 3000 (Thermo Fisher Scientific). Cells were transfected with 1250 ng of a Cas9 base editor expression vector and with 1250 ng of a sgRNA expression vector containing a puromycin-resistance gene. The sgRNA expression vector was generated as follows: A puromycin-resistance gene was PCR amplified from the pSpCas9(BB)-2A-Puro (PX459) V2.0 plasmid, which was a gift from Feng Zhang (Addgene plasmid 62988), appending an AgeI cut site to the 5′ end of the amplicon. This amplicon was inserted into the pX600-AAV-CMV::NLS-SaCas9-NLS-3xHA-bGHpA plasmid, which was a gift from Feng Zhang (Addgene plasmid 61592), replacing the SaCas9 coding region and resulting in a CMV-driven puromycin-resistance gene. By using In-Fusion cloning (ClonTech), this puromycin-expression cassette was inserted into an EcoRI linearized BPK1520 plasmid, which was a gift from Keith Joung (Addgene plasmid 65777). The pLenti-FNLS-P2A-Puro plasmid used for a portion of the cytosine base editing experiments was a gift from Lukas Dow (Addgene plasmid 110841). The pSI-Target-AID-NG plasmid used for the remaining cytosine base editing experiments was a gift from Osamu Nureki (Addgene plasmid 119861). The pCMV_ABEmax_P2A_GFP, VRQR-ABEmax, NG-ABEmax plasmids used for adenine base editing experiments were gifts from David Liu (Addgene plasmids 112101, 119811, 124163). To enrich for transfected cells, 24-h post-transfection cells were subjected to 0.8 µg/mL of puromycin for 72 h. Transfected cells were expanded for genomic DNA isolation and limited dilution as previously described (Essletzbichler et al. 2014).

Genomic DNA isolation and PCR

Genomic DNA was isolated using the DNeasy blood and tissue kit (Qiagen) according to the manufacturer's protocol. PCR was performed using DreamTaq polymerase (Thermo Fisher Scientific) according to the manufacturer's protocol.

Estimation of genome editing

PCR amplification from the genomic DNA of a bulk population of edited cells centered on the predicted editing site was performed. These amplicons were PCR purified using a QIAquick PCR purification kit following the manufacturer's protocol (Qiagen) and Sanger sequenced using the forward primer. To test guide efficiency, the Sanger sequencing files from unedited and edited cells were used as an input into the online sequence trace decomposition software, TIDE (Brinkman et al. 2014). To ascertain base editing percentage, the Sanger sequencing AB1 files were input into the online base editing analysis software, editR (Kluesner et al. 2018).

Protein isolation and western blot analysis

HAP1 cells were trypsinized from their well, pelleted, and washed three times with 1× PBS (Gibco). Protein was isolated from HAP1 cells by resuspending in 150 µL of a one-to-one solution of RIPA homogenizing buffer (50 mM Tris HCl at pH 7.4, 150 nM NaCl, 1-mM EDTA) and RIPA double-detergent buffer (2% deoxycholate, 2% NP-40, 2% Triton X-100 in RIPA homogenizing buffer) supplemented with a protease-inhibitor cocktail (Roche). Cells were subsequently incubated on ice for 30 min. Cells were then centrifuged at 12,000*g* for 15 min at 4°C, and the supernatant was collected and stored at −80°C. Whole-protein concentration was measured using a Pierce BCA protein assay kit according to the manufacturer's protocol (Thermo Fisher Scientific). SDS-Page separation was completed by running 2 µg of total protein on a NuPAGE 3%–8% Tris-acetate gel (Thermo Fisher Scientific). Next, proteins were transferred to a nitrocellulose membrane using the iBlot 2 transfer apparatus (Thermo Fisher Scientific). A 5% milk solution in 1× TBST was used for blocking for 1 h at room temperature. The membrane was then incubated with the NPC1 primary antibody (Abcam ab106534 in main body figures or Novus Biologicals H00004864-M02 in Supplemental Fig. S4) overnight at 4°C. Primary antibody solution was removed, and the membrane was washed three times with 1× TBST. This was followed by a 1-h incubation at room temperature with horseradish peroxidase conjugated goat anti-rabbit IgG (Abcam: ab6721). After three washes with 1× TBST, signal detection was achieved using SuperSignal West Femto Maximum Sensitivity Substrate (Thermo Fisher Scientific) according to the manufacturer's protocol.

Filipin staining

Coverslips were incubated for 1 h at 37°C in 1 mL of 1:30 solution of collagen I rat protein (Thermo Fisher Scientific) to 1× PBS. The collagen solution was then aspirated, and 250,000 HAP1 cells were seeded onto the coverslips in 12-well plate 24 h before staining. Cells were washed three times with 1× PBS and then fixed in 4% paraformaldehyde in 1× PBS for 30 min at room temperature. After fixation, cells were washed three times in 1× PBS and then stained with 50 μg/mL of filipin III (Sigma-Aldrich) for 1 h at room temperature. Coverslips were then washed three times in 1× PBS and mounted onto a slide using ProLong Gold Antifade Mountant (Thermo Fisher Scientific). Cells were visualized using the Zeiss Axiovert 200M epifluorescent microscope, and images were captured with a Hamamatsu C4742-80-12AG camera.

RNA isolation and quantitative PCR

Cells were harvested, washed three times with 1× PBS, pelleted, and then resuspended in TRIzol reagent (Thermo Fisher Scientific). Isolation of mRNA was isolated following the manufacturer's protocol. Next, 500 ng of mRNA was reverse transcribed using SuperScript III reverse transcriptase (Thermo Fisher Scientific) following the manufacturer's protocol. Quantitative PCR using fast SYBR Green master mix (Qiagen) on a StepOnePlus real-time PCR (Applied Biosystems) was performed. *NPC1* expression was analyzed by amplification using a forward primer spanning the junction of exon 12 and 13 and using a reverse primer specific to exon 13. Primers against endogenous *GAPDH* were used as an internal control. ΔΔCt was analyzed to assess fold changes between edited and unedited samples.

RNA sequencing and off-target analysis

RNA sequencing was performed by the Centre for Applied Genomics in Toronto using the Illumina HiSeq 2500 system, producing 120-bp paired-end reads. Raw transcript reads were aligned to the GRCh38 human genome using HISAT2 (Kim et al. 2015). The Picard program (v2.21.1; http://broadinstitute.github.io/picard) was used to mark duplicative and sort reads. The Genome Analysis Toolkit (GATK; v4.1.3.0) (Poplin et al. 2018) was used to split the reads that contained Ns in their CIGAR string (McKenna et al. 2010). Variant calling was conducted with both FreeBayes (v1.3.1) and LoFreq (v2.1.3) independently (Garrison and Marth 2012; Wilm et al. 2012). Only variants called by both software programs were considered true variants. Any variants with a read depth of less than four, or an allele frequency less than 0.4, were filtered from the final list of unique mutant variants. The exon coordinates of GRCh38 version 86 were retrieved from the Ensembl database (Hunt et al. 2018), and any called variants falling outside of these coordinates were excluded. The final list of variants was manually inspected using the Integrative Genomics Viewer (IGV) software (Thorvaldsdottir et al. 2013).

Statistical analyses

All graphs were plotted as the mean with error bars indicating standard error. Differences between groups was assessed by two-tailed Student's *t*-test. *P*-values < 0.05 were considered statistically significant.

Data access

All sgRNA and primer sequences are available in Supplemental Table S2. The sequencing data generated in this study have been submitted to the NCBI BioProject database (https://www.ncbi.nlm.nih.gov/bioproject) under accession number PRJNA580451.

Acknowledgments

We thank Niemann–Pick Canada and the Marcogliese Family Foundation for their support and commitment to our research into Niemann–Pick disease type C. We thank Ebony Thompson, Sonia Evagelou, and Kyle Lindsay for their technical assistance. Figure 2A was created with Biorender.com. This work was supported by the Rare Disease Foundation and the BC Children's Hospital Foundation (2304 to S.E.), The Hospital for Sick Children (Restracomp scholarship to S.E.), Niemann Pick Canada, and the Marcogliese Family Foundation.

Author contributions: Conceptualization was by S.E., E.A.I., and R.D.C. Methodology was by S.E., R.A.B., T.M.I.B., E.M., L.Z., E.A.I., and R.D.C. Formal analysis was by S.E., R.A.B., T.M.I.B., E.A.I., and R.D.C. Investigation was by S.E., R.A.B., T.M.I.B., E.M., E.A.I., and R.D.C. Resources were by E.A.I. and R.D.C. Data curation was by S.E., R.A.B., T.M.I.B., E.A.I., and R.D.C. Writing, original draft preparation, was by S.E. Writing, review and editing, was by S.E., R.A.B., T.M.I.B., E.M., L.Z., E.A.I., and R.D.C. Supervision was by E.A.I. and R.D.C. Project administration was by E.A.I. and R.D.C. Funding acquisition was by S.E., E.A.I., and R.D.C.

References

Brinkman EK, Chen T, Amendola M, van Steensel B. 2014. Easy quantitative assessment of genome editing by sequence trace decomposition. *Nucleic Acids Res* **42:** e168. doi:10.1093/nar/gku936

Carette JE, Raaben M, Wong AC, Herbert AS, Obernosterer G, Mulherkar N, Kuehne AI, Kranzusch PJ, Griffin AM, Ruthel G, et al. 2011. Ebola virus entry requires the cholesterol transporter Niemann–Pick C1. *Nature* **477:** 340–343. doi:10.1038/nature10348

Cho SW, Kim S, Kim JM, Kim JS. 2013. Targeted genome engineering in human cells with the Cas9 RNA-guided endonuclease. *Nat Biotechnol* **31:** 230–232. doi:10.1038/nbt.2507

Davies JP, Ioannou YA. 2000. Topological analysis of Niemann–Pick C1 protein reveals that the membrane orientation of the putative sterol-sensing domain is identical to those of 3-hydroxy-3-methylglutaryl-CoA reductase and sterol regulatory element binding protein cleavage-activating protein. *J Biol Chem* **275:** 24367–24374. doi:10.1074/jbc.M002184200

Du X, Lukmantara I, Yang H. 2017. CRISPR/Cas9-mediated generation of Niemann–Pick C1 knockout cell line. *Methods Mol Biol* **1583:** 73–83. doi:10.1007/978-1-4939-6875-6_7

Essletzbichler P, Konopka T, Santoro F, Chen D, Gapp BV, Kralovics R, Brummelkamp TR, Nijman SM, Bürckstummer T. 2014. Megabase-scale deletion using CRISPR/Cas9 to generate a fully haploid human cell line. *Genome Res* **24:** 2059–2065. doi:10.1101/gr.177220.114

Fernandez-Valero EM, Ballart A, Iturriaga C, Lluch M, Macias J, Vanier MT, Pineda M, Coll MJ. 2005. Identification of 25 new mutations in 40 unrelated Spanish Niemann–Pick type C patients: genotype-phenotype correlations. *Clin Genet* **68:** 245–254. doi:10.1111/j.1399-0004.2005.00490.x

Findlay GM, Daza RM, Martin B, Zhang MD, Leith AP, Gasperini M, Janizek JD, Huang X, Starita LM, Shendure J. 2018. Accurate classification of *BRCA1* variants with saturation genome editing. *Nature* **562:** 217–222. doi:10.1038/s41586-018-0461-z

Frischmeyer PA, Dietz HC. 1999. Nonsense-mediated mRNA decay in health and disease. *Hum Mol Genet* **8:** 1893–1900. doi:10.1093/hmg/8.10.1893

Garrison E, Marth G. 2012. Haplotype-based variant detection from short-read sequencing. arXiv:1207.3907 [q-bio.GN].

Gaudelli NM, Komor AC, Rees HA, Packer MS, Badran AH, Bryson DI, Liu DR. 2017. Programmable base editing of A•T to G•C in genomic DNA without DNA cleavage. *Nature* **551:** 464–471. doi:10.1038/nature24644

Gelsthorpe ME, Baumann N, Millard E, Gale SE, Langmade SJ, Schaffer JE, Ory DS. 2008. Niemann–Pick type C1 I1061T mutant encodes a functional protein that is selected for endoplasmic reticulum-associated degradation due to protein misfolding. *J Biol Chem* **283:** 8229–8236. doi:10.1074/jbc.M708735200

Greer WL, Dobson MJ, Girouard GS, Byers DM, Riddell DC, Neumann PE. 1999. Mutations in NPC1 highlight a conserved NPC1-specific cysteine-rich domain. *Am J Hum Genet* **65:** 1252–1260. doi:10.1086/302620

Hess GT, Frésard L, Han K, Lee CH, Li A, Cimprich KA, Montgomery SB, Bassik MC. 2016. Directed evolution using dCas9-targeted somatic hypermutation in mammalian cells. *Nat Methods* **13:** 1036–1042. doi:10.1038/nmeth.4038

Hu JH, Miller SM, Geurts MH, Tang W, Chen L, Sun N, Zeina CM, Gao X, Rees HA, Lin Z, et al. 2018. Evolved Cas9 variants with broad PAM compatibility and high DNA specificity. *Nature* **556:** 57–63. doi:10.1038/nature26155

Hua K, Tao X, Zhu JK. 2019. Expanding the base editing scope in rice by using Cas9 variants. *Plant Biotechnol J* **17:** 499–504. doi:10.1111/pbi.12993

Huang TP, Zhao KT, Miller SM, Gaudelli NM, Oakes BL, Fellmann C, Savage DF, Liu DR. 2019. Circularly permuted and PAM-modified Cas9 variants broaden the targeting scope of base editors. *Nat Biotechnol* **37:** 626–631. doi:10.1038/s41587-019-0134-y

Hunt SE, McLaren W, Gil L, Thormann A, Schuilenburg H, Sheppard D, Parton A, Armean IM, Trevanion SJ, Flicek P, et al. 2018. Ensembl variation resources. *Database* **2018:** bay119. doi:10.1093/database/bay119

Jin S, Zong Y, Gao Q, Zhu Z, Wang Y, Qin P, Liang C, Wang D, Qiu JL, Zhang F, et al. 2019. Cytosine, but not adenine, base editors induce genome-wide off-target mutations in rice. *Science* **364:** 292–295. doi:10.1126/science.aaw7166

Jinek M, Chylinski K, Fonfara I, Hauer M, Doudna JA, Charpentier E. 2012. A programmable dual-RNA–guided DNA endonuclease in adaptive bacterial immunity. *Science* **337:** 816–821. doi:10.1126/science.1225829

Kim D, Langmead B, Salzberg SL. 2015. HISAT: a fast spliced aligner with low memory requirements. *Nat Methods* **12:** 357–360. doi:10.1038/nmeth.3317

Kim HS, Jeong YK, Hur JK, Kim JS, Bae S. 2019. Adenine base editors catalyze cytosine conversions in human cells. *Nat Biotechnol* **37:** 1145–1148. doi:10.1038/s41587-019-0254-4

Kluesner MG, Nedveck DA, Lahr WS, Garbe JR, Abrahante JE, Webber BR, Moriarity BS. 2018. EditR: a method to quantify base editing from Sanger sequencing. *CRISPR J* **1:** 239–250. doi:10.1089/crispr.2018.0014

Koblan LW, Doman JL, Wilson C, Levy JM, Tay T, Newby GA, Maianti JP, Raguram A, Liu DR. 2018. Improving cytidine and adenine base editors by expression optimization and ancestral reconstruction. *Nat Biotechnol* **36:** 843–846. doi:10.1038/nbt.4172

Komor AC, Kim YB, Packer MS, Zuris JA, Liu DR. 2016. Programmable editing of a target base in genomic DNA without double-stranded DNA cleavage. *Nature* **533:** 420–424. doi:10.1038/nature17946

Komor AC, Zhao KT, Packer MS, Gaudelli NM, Waterbury AL, Koblan LW, Kim YB, Badran AH, Liu DR. 2017. Improved base excision repair inhibition and bacteriophage Mu Gam protein yields C:G-to-T:A base editors with higher efficiency and product purity. *Sci Adv* **3:** eaao4774. doi:10.1126/sciadv.aao4774

Landrum MJ, Lee JM, Riley GR, Jang W, Rubinstein WS, Church DM, Maglott DR. 2014. ClinVar: public archive of relationships among sequence variation and human phenotype. *Nucleic Acids Res* **42:** D980–D985. doi:10.1093/nar/gkt1113

Landrum MJ, Lee JM, Benson M, Brown G, Chao C, Chitipiralla S, Gu B, Hart J, Hoffman D, Hoover J, et al. 2016. ClinVar: public archive of interpretations of clinically relevant variants. *Nucleic Acids Res* **44:** D862–D868. doi:10.1093/nar/gkv1222

Lek M, Karczewski KJ, Minikel EV, Samocha KE, Banks E, Fennell T, O'Donnell-Luria AH, Ware JS, Hill AJ, Cummings BB, et al. 2016. Analysis of protein-coding genetic variation in 60,706 humans. *Nature* **536:** 285–291. doi:10.1038/nature19057

Li X, Lu F, Trinh MN, Schmiege P, Seemann J, Wang J, Blobel G. 2017. 3.3 Å structure of Niemann–Pick C1 protein reveals insights into the function of the C-terminal luminal domain in cholesterol transport. *Proc Natl Acad Sci* **114:** 9116–9121. doi:10.1073/pnas.1711716114

Ma Y, Zhang J, Yin W, Zhang Z, Song Y, Chang X. 2016. Targeted AID-mediated mutagenesis (TAM) enables efficient genomic diversification in mammalian cells. *Nat Methods* **13:** 1029–1035. doi:10.1038/nmeth.4027

Macias-Vidal J, Gort L, Lluch M, Pineda M, Coll MJ. 2009. Nonsense-mediated mRNA decay process in nine alleles of Niemann–Pick type C patients from Spain. *Mol Genet Metab* **97:** 60–64. doi:10.1016/j.ymgme.2009.01.007

Mali P, Esvelt KM, Church GM. 2013a. Cas9 as a versatile tool for engineering biology. *Nat Methods* **10:** 957–963. doi:10.1038/nmeth.2649

Mali P, Yang L, Esvelt KM, Aach J, Guell M, DiCarlo JE, Norville JE, Church GM. 2013b. RNA-guided human genome engineering via Cas9. *Science* **339:** 823–826. doi:10.1126/science.1232033

McKay Bounford K, Gissen P. 2014. Genetic and laboratory diagnostic approach in Niemann Pick disease type C. *J Neurol* **261:** S569–S575. doi:10.1007/s00415-014-7386-8

McKenna A, Hanna M, Banks E, Sivachenko A, Cibulskis K, Kernytsky A, Garimella K, Altshuler D, Gabriel S, Daly M, et al. 2010. The Genome Analysis Toolkit: a MapReduce framework for analyzing next-generation DNA sequencing data. *Genome Res* **20:** 1297–1303. doi:10.1101/gr.107524.110

Millat G, Marçais C, Tomasetto C, Chikh K, Fensom AH, Harzer K, Wenger DA, Ohno K, Vanier MT. 2001. Niemann–Pick C1 disease: Correlations between *NPC1* mutations, levels of NPC1 protein, and phenotypes emphasize the functional significance of the putative sterol-sensing domain and of the cysteine-rich luminal loop. *Am J Hum Genet* **68:** 1373–1385. doi:10.1086/320606

Nakasone N, Nakamura YS, Higaki K, Oumi N, Ohno K, Ninomiya H. 2014. Endoplasmic reticulum-associated degradation of Niemann–Pick C1: evidence for the role of heat shock proteins and identification of lysine residues that accept ubiquitin. *J Biol Chem* **289:** 19714–19725. doi:10.1074/jbc.M114.549915

Nishimasu H, Ran FA, Hsu PD, Konermann S, Shehata SI, Dohmae N, Ishitani R, Zhang F, Nureki O. 2014. Crystal structure of Cas9 in complex with guide RNA and target DNA. *Cell* **156:** 935–949. doi:10.1016/j.cell.2014.02.001

Nishimasu H, Shi X, Ishiguro S, Gao L, Hirano S, Okazaki S, Noda T, Abudayyeh OO, Gootenberg JS, Mori H, et al. 2018. Engineered CRISPR-Cas9 nuclease with expanded targeting space. *Science* **361:** 1259–1262. doi:10.1126/science.aas9129

Ory DS. 2000. Niemann–Pick type C: a disorder of cellular cholesterol trafficking. *Biochim Biophys Acta* **1529:** 331–339. doi:10.1016/S1388-1981(00)00158-X

Park WD, O'Brien JF, Lundquist PA, Kraft DL, Vockley CW, Karnes PS, Patterson MC, Snow K. 2003. Identification of 58 novel mutations in Niemann–Pick disease type C: correlation with biochemical phenotype and importance of *PTC1*-like domains in *NPC1*. *Hum Mutat* **22:** 313–325. doi:10.1002/humu.10255

Patterson MC, Mengel E, Wijburg FA, Muller A, Schwierin B, Drevon H, Vanier MT, Pineda M. 2013. Disease and patient characteristics in NP-C patients: findings from an international disease registry. *Orphanet J Rare Dis* **8:** 12. doi:10.1186/1750-1172-8-12

Poplin R, Ruano-Rubio V, DePristo MA, Fennell TJ, Carneiro MO, Van der Auwera GA, Kling DE, Gauthier LD, Levy-Moonshine A, Roazen D, et al. 2018. Scaling accurate genetic variant discovery to tens of thousands of samples. bioRxiv doi:10.1101/201178

Rauniyar N, Subramanian K, Lavallee-Adam M, Martinez-Bartolomé S, Balch WE, Yates JR 3rd. 2015. Quantitative proteomics of human fibroblasts with I1061T mutation in Niemann–Pick C1 (NPC1) protein provides insights into the disease pathogenesis. *Mol Cell Proteomics* **14:** 1734–1749. doi:10.1074/mcp.M114.045609

Rees HA, Liu DR. 2018. Base editing: precision chemistry on the genome and transcriptome of living cells. *Nat Rev Genet* **19:** 770–788. doi:10.1038/s41576-018-0059-1

Rees HA, Komor AC, Yeh WH, Caetano-Lopes J, Warman M, Edge ASB, Liu DR. 2017. Improving the DNA specificity and applicability of base editing through protein engineering and protein delivery. *Nat Commun* **8:** 15790. doi:10.1038/ncomms15790

Richards S, Aziz N, Bale S, Bick D, Das S, Gastier-Foster J, Grody WW, Hegde M, Lyon E, Spector E, et al. 2015. Standards and guidelines for the interpretation of sequence variants: a joint consensus recommendation of the American College of Medical Genetics and Genomics and the Association for Molecular Pathology. *Genet Med* **17:** 405–424. doi:10.1038/gim.2015.30

Rodriguez-Pascau L, Coll MJ, Casas J, Vilageliu L, Grinberg D. 2012. Generation of a human neuronal stable cell model for Niemann–Pick C disease by RNA interference. *JIMD Rep* **4:** 29–37. doi:10.1007/8904_2011_64

Schultz ML, Krus KL, Kaushik S, Dang D, Chopra R, Qi L, Shakkottai VG, Cuervo AM, Lieberman AP. 2018. Coordinate regulation of mutant NPC1 degradation by selective ER autophagy and MARCH6-dependent ERAD. *Nat Commun* **9:** 3671. doi:10.1038/s41467-018-06115-2

Scott C, Ioannou YA. 2004. The NPC1 protein: structure implies function. *Biochim Biophys Acta* **1685:** 8–13. doi:10.1016/j.bbalip.2004.08.006

Tan J, Zhang F, Karcher D, Bock R. 2019. Engineering of high-precision base editors for site-specific single nucleotide replacement. *Nat Commun* **10:** 439. doi:10.1038/s41467-018-08034-8

Tarugi P, Ballarini G, Bembi B, Battisti C, Palmeri S, Panzani F, Di Leo E, Martini C, Federico A, Calandra S. 2002. Niemann–Pick type C disease: mutations of NPC1 gene and evidence of abnormal expression of some mutant alleles in fibroblasts. *J Lipid Res* **43:** 1908–1919. doi:10.1194/jlr.M200203-JLR200

Tharkeshwar AK, Trekker J, Vermeire W, Pauwels J, Sannerud R, Priestman DA, te Vruchte D, Vints K, Baatsen P, Decuypere JP, et al. 2017. A novel approach to analyze lysosomal dysfunctions through subcellular proteomics and lipidomics: the case of NPC1 deficiency. *Sci Rep* **7:** 41408. doi:10.1038/srep41408

Thorvaldsdottir H, Robinson JT, Mesirov JP. 2013. Integrative Genomics Viewer (IGV): high-performance genomics data visualization and exploration. *Brief Bioinform* **14:** 178–192. doi:10.1093/bib/bbs017

Vanier MT. 2010. Niemann–Pick disease type C. *Orphanet J Rare Dis* **5:** 16. doi:10.1186/1750-1172-5-16

Vanier MT, Rodriguez-Lafrasse C, Rousson R, Gazzah N, Juge MC, Pentchev PG, Revol A, Louisot P. 1991. Type C Niemann–Pick disease: spectrum of phenotypic variation in disruption of intracellular LDL-derived cholesterol processing. *Biochim Biophys Acta* **1096:** 328–337. doi:10.1016/0925-4439(91)90069-L

Wassif CA, Cross JL, Iben J, Sanchez-Pulido L, Cougnoux A, Platt FM, Ory DS, Ponting CP, Bailey-Wilson JE, Biesecker LG, et al. 2016. High incidence of unrecognized visceral/neurological late-onset Niemann–Pick disease, type C1, predicted by analysis of massively parallel sequencing data sets. *Genet Med* **18:** 41–48. doi:10.1038/gim.2015.25

Watari H, Blanchette-Mackie EJ, Dwyer NK, Watari M, Neufeld EB, Patel S, Pentchev PG, Strauss JF 3rd. 1999. Mutations in the leucine zipper motif and sterol-sensing domain inactivate the Niemann–Pick C1 glycoprotein. *J Biol Chem* **274:** 21861–21866. doi:10.1074/jbc.274.31.21861

Wilm A, Aw PP, Bertrand D, Yeo GH, Ong SH, Wong CH, Khor CC, Petric R, Hibberd ML, Nagarajan N. 2012. LoFreq: a sequence-quality aware, ultra-sensitive variant caller for uncovering cell-population heterogeneity from high-throughput sequencing datasets. *Nucleic Acids Res* **40:** 11189–11201. doi:10.1093/nar/gks918

Wojtanik KM, Liscum L. 2003. The transport of low density lipoprotein-derived cholesterol to the plasma membrane is defective in NPC1 cells. *J Biol Chem* **278:** 14850–14856. doi:10.1074/jbc.M300488200

Yamamoto T, Ninomiya H, Matsumoto M, Ohta Y, Nanba E, Tsutsumi Y, Yamakawa K, Millat G, Vanier MT, Pentchev PG, et al. 2000. Genotype-phenotype relationship of Niemann–Pick disease type C: a possible correlation between clinical onset and levels of NPC1 protein in isolated skin fibroblasts. *J Med Genet* **37:** 707–712. doi:10.1136/jmg.37.9.707

Yamamoto T, Feng JH, Higaki K, Taniguchi M, Nanba E, Ninomiya H, Ohno K. 2004. Increased *NPC1* mRNA in skin fibroblasts from Niemann–Pick disease type C patients. *Brain Dev* **26:** 245–250. doi:10.1016/S0387-7604(03)00162-1

Yang L, Zhang X, Wang L, Yin S, Zhu B, Xie L, Duan Q, Hu H, Zheng R, Wei Y, et al. 2018. Increasing targeting scope of adenosine base editors in mouse and rat embryos through fusion of TadA deaminase with Cas9 variants. *Protein Cell* **9:** 814–819. doi:10.1007/s13238-018-0568-x

Yasui M, Suenaga E, Koyama N, Masutani C, Hanaoka F, Gruz P, Shibutani S, Nohmi T, Hayashi M, Honma M. 2008. Miscoding properties of 2′-deoxyinosine, a nitric oxide-derived DNA adduct, during translesion synthesis catalyzed by human DNA polymerases. *J Mol Biol* **377:** 1015–1023. doi:10.1016/j.jmb.2008.01.033

Zafra MP, Schatoff EM, Katti A, Foronda M, Breinig M, Schweitzer AY, Simon A, Han T, Goswami S, Montgomery E, et al. 2018. Optimized base editors enable efficient editing in cells, organoids and mice. *Nat Biotechnol* **36:** 888–893. doi:10.1038/nbt.4194

Zampieri S, Bembi B, Rosso N, Filocamo M, Dardis A. 2012. Treatment of human fibroblasts carrying NPC1 missense mutations with MG132 leads to an improvement of intracellular cholesterol trafficking. *JIMD Rep* **2:** 59–69. doi:10.1007/8904_2011_49

Zhao K, Ridgway ND. 2017. Oxysterol-binding protein-related protein 1L regulates cholesterol egress from the endo-lysosomal system. *Cell Rep* **19:** 1807–1818. doi:10.1016/j.celrep.2017.05.028

Zuo E, Sun Y, Wei W, Yuan T, Ying W, Sun H, Yuan L, Steinmetz LM, Li Y, Yang H. 2019. Cytosine base editor generates substantial off-target single-nucleotide variants in mouse embryos. *Science* **364:** 289–292. doi:10.1126/science.aav9973

Received March 20, 2019; accepted in revised form November 1, 2019.